Research Article

Nano Biomed Eng

A Device for the Removal of Peripheral Blood Circulating Tumor Cells and Inhibiting Their Biodistribution

Jun Luo[1,§], Lei Xing[1,3,§], Ming-Tao Yu[1,§], Ying Sun[1], Wen-Jia Wang[1], Xing Wan[1], Xiao-Jie Wang[1], Yang-Ze Ji[1], Yi Wang[1], Tian-Jiao Zhou[1], Hu-Lin Jiang[1,2,3]✉

[1] State Key Laboratory of Natural Medicines, Department of Pharmaceutics, China Pharmaceutical University, Nanjing 210009, China

[2] Department of Precision Medicine, School of Medicine, Sungkyunkwan University, Suwon 16419, Republic of Korea

[3] NMPA Key Laboratory for Research and Evaluation of Pharmaceutical Preparations and Excipients, China Pharmaceutical University, Nanjing 210009, China

[§] These authors contributed equally to this work.

✉ Corresponding author. E-mail: jianghulin3@gmail.com, jianghulin3@163.com

Received: Dec. 6, 2024; **Revised:** Jan. 13, 2025; **Accepted:** Jan. 15, 2025

Citation: J. Luo, L. Xing, M.-T. Yu, et al. A device for the removal of peripheral blood circulating tumor cells and inhibiting their biodistribution. *Nano Biomedicine and Engineering*, 2025, 17(3): 386−401.

http://doi.org/10.26599/NBE.2025.9290114

Abstract

Circulating tumor cells (CTCs) significantly impact the overall survival and progression-free survival of cancer patients. However, the current strategies for CTC separation and enrichment are limited as they analyze only small-volume blood samples, which is insufficient to comprehensively profile the distribution of CTCs in the blood and eliminate them. To address this issue, we developed a peripheral blood CTC removal device (PBCRD) inspired by hemoperfusion. It comprises systems for CTC-capturing and returning purified blood into circulation. The CTC capturing system consists of antibody-modified functional microspheres (AFMPs), while the purified blood returning system includes a peristaltic circulation pump for clinical blood perfusion and catheters. The PBCRD can efficiently capture, enrich, and remove CTCs from peripheral circulation in real-time, effectively inhibiting their biodistribution. The high biocompatibility of AFMPs ensures that PBCRD is safe and does not cause injuries. Overall, this work provides a new class of ideas for the effective capture and removal of CTCs from the peripheral circulation, which is expected to be an effective strategy to assist in the clinical treatment of tumors and inhibit metastasis.

Keywords: circulating tumor cells; blood purification system; epithelial cell adhesion molecules antibody; capture device; tumor metastasis

Introduction

At present, cancer is a serious public health care threat that needs urgent resolution [1]. More than 90% of cancer-related deaths are caused by tumor invasion and metastasis [2, 3], and the 5-year relative survival rate of patients with metastatic cancer is considerably lower than that of patients with localized cancer [4]. Since the concept of circulating tumor cells (CTCs) was first proposed in 1896 [5], the shedding of CTCs from the primary tumor and their entry into the blood or lymph circulation, arrival at

the metastatic focus, cloning, and proliferation have been widely recognized as the components of the primary mechanism underlying cancer metastasis [6–8]. The CTC number is closely associated with an unfavorable prognosis in most cancers [9, 10]. Therefore, the detection, separation, and numeration of CTCs have played crucial roles in providing insights into cancer progression and guiding clinical medication [5, 11].

To date, several kinds of immunomagnetic affinity-based beads, multifunctional microfluidic chips, and functional nanomaterials have been exploited for the enrichment and separation of CTCs [12–19]. To capture CTCs in pure blood, a capture device can be designed based on the differences in size, density, deformability, adhesion, and biomarkers of CTCs and peripheral blood cells [20–26]. Using antibody/aptamer-modified immune magnetic beads [27–30], multifunctional microfluidic chips, or a combination of both can effectively capture CTCs in pure blood [31–34]. Similarly, the combination of microfluidic chips and indwelling catheters has further succeeded in capturing CTCs from peripheral blood circulation [35–38]. These methods have enhanced the capture of CTCs from the peripheral circulation to a certain extent. However, they are inadequate for the real-time capture of CTCs from large volumes of blood, especially in samples obtained from the peripheral circulation, due to limitations in the sample volume utilized. Additionally, as CTCs are very rare in the blood circulation of cancer patients, and the peripheral blood contains numerous red blood (RBCs) and immune cells [39], it is difficult to capture the tumor cells hidden in the bloodstream with high specificity [40–42]. Therefore, trapping CTCs from the peripheral circulation with enhanced specificity and removing them from patients is a vital problem and a promising clinical treatment for tumor recurrence and metastasis.

Inspired by the ability of blood purification systems to remove metabolic wastes and toxins from the blood [43, 44], we employed the highly biocompatible hemoperfusion adsorbent antibody-modified functional microspheres (AFMPs), which targets modified antibodies for CTC capture, enrichment, and removal from blood (Fig. 1). We combined the AFMPs with a purified blood circulation system to establish a novel Peripheral Blood CTC Removal Device (PBCRD) utilizing the blood perfusion mode to extract the blood containing CTCs from the body and capture the CTCs in the blood with the use of antiepithelial cell adhesion molecules (EpCAM) antibody-modified functional microspheres (MPs). As CTCs are known to express EpCAM at elevated levels, the adsorbent surface was grafted with PEG-linked protein G, which has albumin- and an IgG antibody-binding domains at the N- and C-termini, respectively. Through non-specific immunological techniques, protein G can bind to the Fc fragment of the antibody, and then the adsorbent surface is modified with bovine serum albumin (BSA) to resist the physical adsorption of proteins and normal cells from the blood. The novel device achieved the capture, enrichment, and elimination of CTCs in the large volume of circulating peripheral blood. This method is a creative approach to direct blood purification for tumor recurrence and metastasis; a strategy that has great clinical application value in suppressing the probability of tumor metastasis, improving the quality of life of patients, and prolonging the survival time of cancer patients.

Materials and Methods

Materials

The poly(styrene-*co*-divinylbenzene), ion-exchange resin carboxylate microsphere (PS–DVB–COOH) was purchased from the Tianjin HEOWNS Biochemical Technology Co., Ltd, Tianjin, China. Microperistaltic pumps and rubber hoses were purchased from the Kamoer Fluid Tech Co. Ltd., Shanghai, China. 1-ethyl-3-(3-[dimethylamino] propyl) carbodiimide hydrochloride (EDC), N-hydroxysuccinimide (NHS), bovine serum albumin (BSA; free of reactive sulfhydryl groups), FITC-PEG-maleimde (5 kDa), and 2-iminothiolane (Traut's Reagent) were purchased from Aladdin Chemistry (Shanghai, China). Recombinant protein G and 1,1'-Dioctadecyl-3,3,3',3'-tetramethylindodicarbocyanine, 4-chlorobenzenesulfonate salt (DiD) were purchased from Beyotime Biotech Inc., Jiangsu, China. Maleimide PEG Amine (NH_2–PEG–Mal; 5 kDa) was purchased from Hangzhou Ready Biological Technology Co., Ltd., Hangzhou, China. The antihuman EpCAM antibody was purchased from R&D Systems, MN, USA. Alexa Fluor®647-conjugated EpCAM mouse mAb and FITC-

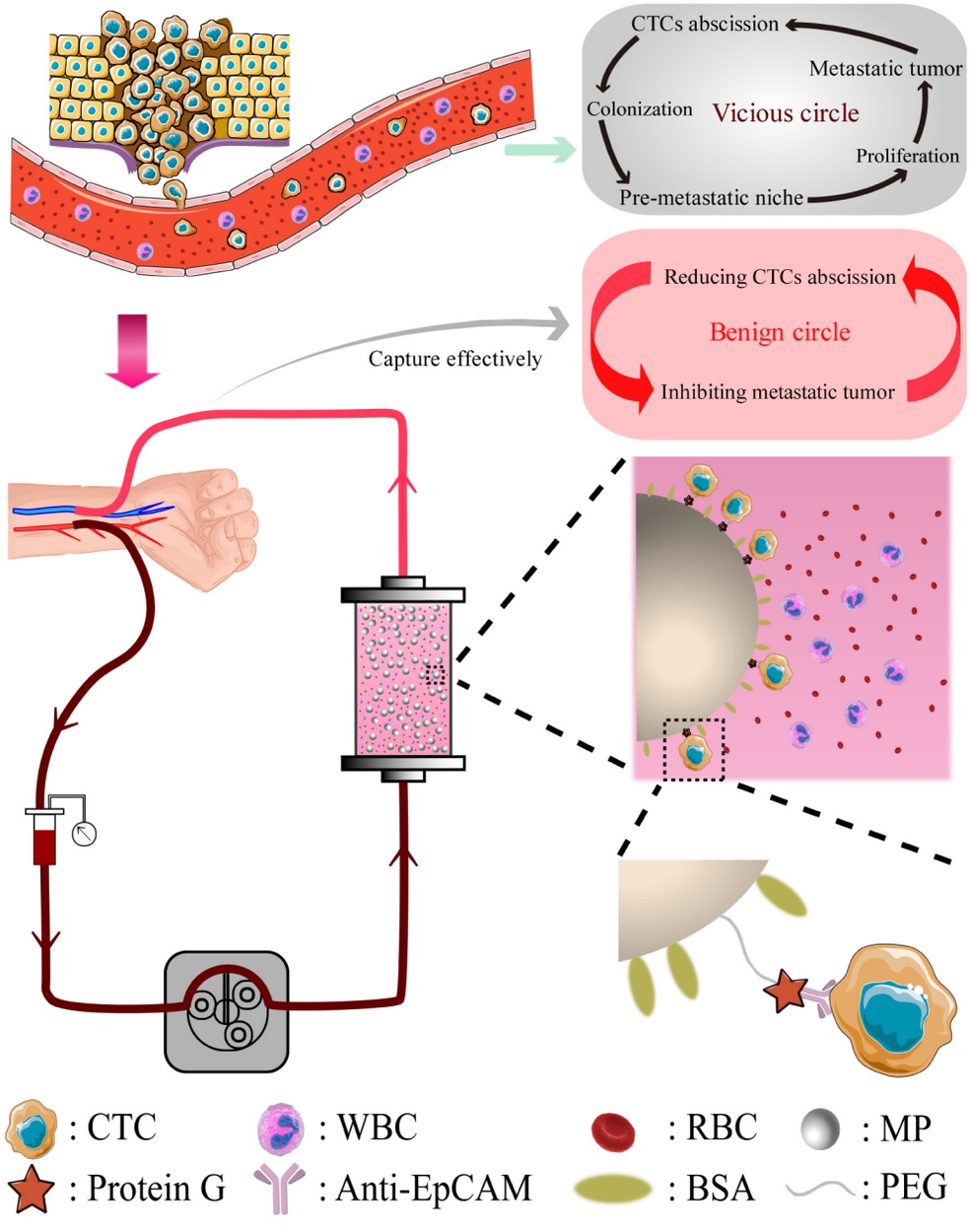

Fig. 1 Schematic diagram of the hemoperfusion and capturing CTC process.

conjugated EpCAM mouse mAb were purchased from Santa Cruz Biotechnology, TX, USA. Dulbecco's modified Eagle's medium (DMEM) and the Roswell Park Memorial Institute 1640 (RPMI-1640) medium were purchased from Jiangsu KeyGEN Biotech Co., Ltd. Jiangsu, China. Fetal bovine serum (FBS) was obtained from Gibco, MA, USA. The phosphate buffer was self-prepared. The water utilized in all experiments was purified by a Milli-Q Plus 185 water purification system from Millipore, MA, USA.

Conjugation of Protein G to NH_2–PEG–MAL

Protein G and Traut's Reagent, 2 mg each, were coincubated in 1 mL of PBS for 45 min at room temperature. The reaction solution was centrifugally purified on Sephadex microcolumns to collect the thiolated protein G. NH_2–PEG–Mal, 2 mg was coincubated with the thiolated protein G solution for 4 h at room temperature. The solution was then purified utilizing a dialysis bag (10 kDa) to remove the free NH_2–PEG–Mal. The purified PG–PEG–Mal solution was stored at 4 °C before use.

Preparation of the functionalized adsorbents

The unmodified MPs (50 mg) were reacted with the NHS–EDC solution for 15 min at room temperature to activate the -COOH groups on the MP surface. Then, the MPs were incubated with PG–PEG–Mal overnight at 37 °C. The nonspecific binding sites were blocked with 5%BSA overnight at 4 °C to resist

physical adsorption (AMP). After washing with PBS thrice, the AMP was treated with 5 μg·mL^{-1} anti-EpCAM antibody solution overnight at 37 °C (AFMP). After washing with PBS, the functionalized MPs were stored at 4 °C before use.

Cell culture

Human lung adenocarcinoma H1975 cells and human cervical cancer HeLa cells were purchased from the American type culture collection. H1975 cells were cultured in RPMI 1640 medium, and HeLa cells in DMEM medium, which was supplemented with 10% (v·v^{-1}) FBS and 100 U·mL^{-1} each of penicillin and streptomycin at 37 °C and under 5%CO_2.

PBCRD-based CTC capture experiments

An extracorporeal simulated circulatory system was constructed to verify the capability of AFMP-capturing tumor cells. It was composed of a microperistaltic pump that provided hemodynamic force, a 4.8 mm rubber hose, and a blood perfusion device. H1975 cells were further selected as model cells to verify the CTC capture ability of the blood perfusion device. They were stained with DiD before being spiked into the circulatory system. After allowing circulation for 30 min, the functionalized MPs were washed with PBS thrice and monitored under a laser confocal scanning microscope (CLSM).

First, the tumor cell capture efficiency of the PBCRD device was investigated at different times. For this, 1 × 10^6 H1975 cells were injected into a centrifuge tube and the circulation was turned on for 15, 20, 25, 30, or 25 min. The tumor cell capture efficiency was then calculated. To ascertain the optimal capture speed of the blood purifier device, 1 × 10^6 H1975 cells were spiked into a centrifuge tube containing 10 mL of PBS and circulated under flow velocities of 5, 10, 15, 20, or 25 mL·min^{-1} for 30 min. Then, the H1975 cell suspension in the circulation pipeline was removed and counted after centrifugal resuspension.

To verify the ability of the blood purifier device to capture CTCs in the simulated blood environment, RPMI 1640 medium with 55% FBS was utilized as the circulating medium to simulate the blood viscosity and immune environment. For this, 1 × 10^6 H1975 cells were spiked into the medium and circulated for 30 min, and the cells were counted after centrifugal resuspension.

In vivo extracorporeal blood circulation experiment in a live animal

Adult, male, 3-month-old Sprague-Dawley rats, weighing between 250 and 300 g were used as the experimental animals. The *in vivo* extracorporeal blood circulation experiment was established as follows: the experimental rat was anesthetized and the abdominal skin was cut to separate the abdominal artery and the abdominal main vein. Blood was drawn after cannulation at the artery, allowed to enter the blood perfusion device through the circulation pipeline, exit from the vein, and flow back into the experimental rat. A total of 1 × 10^6 H1975 cells were injected into the tail vein before the start of the cycle, and then the cells were captured during a cycle lasting 30 min. The CTCs were captured by the device when blood flowed through the circulation pipeline.

To prove that the AFMPs could capture CTCs in rat blood circulation, the MPs were removed from circulation after 30 min of the above operation. The cells captured on the MP surface were digested and exfoliated with 1 mL of trypsin. Then, the digestion solution was treated with 10 mL of erythrocyte lysate for 10 min, centrifuged, and concentrated to obtain a mixed suspension of immune and CTC-model cells. The cell suspension was incubated with the FITC-labeled CD45 and Alexa Fluor®647-labeled EpCAM antibodies at 4 °C for 30 min. After centrifugation, the cell suspension was washed thrice with PBS and stained with DAPI for 10 min. The captured cells were observed under CLSM post-treatment.

To verify the capability of the AFMP-capturing tumor cells, H1975 cells were spiked into the circulating medium after DAPI staining. After circulation for 30 min, the rat blood was collected and lysed with the red cell lysis solution to eliminate the RBCs. The remaining resuspended cells were ultrasonically crushed and the fluorescent compound was detected in the suspension.

To confirm the feasibility of inhibiting tumor metastasis *in vivo* after capturing CTCs employing circulatory devices with AFMP, a total of 4 × 10^5 H1975 cells were spiked into the extracorporeal circulation system after DIR staining. After circulation for 30 min, the flowing cell suspension was collected and intravenously injected into the mice after centrifugation and resuspension. The images of the mice were captured with an *in vivo* imaging

system (IVIS) 3 h later after injection. Then, the mice were sacrificed, and the images of the main viscera were captured by IVIS. Simultaneously, the quantitative fluorescence intensity was measured to investigate the retention of H1975 cells in mice and the main viscera.

Statistical analysis

Statistical analyses were performed using GraphPad Prism software (https://www.graphpad.com/features). For all statistical analyses, $n \geq 3$ was employed. All data are presented as mean ± standard deviation (SD), calculated employing the SPSS statistical software (IBM, NY, USA). Intergroup values were compared using a Student's *t*-test. One-way ANOVA with Scheffe's post-hoc multiple comparison tests was applied to compare the variance among multiple groups, with $p < 0.05$ regarded as statistically significant. The differences were considered statistically vital at $*p < 0.05$, $**p < 0.01$, $***p < 0.001$, and $****p < 0.0001$. N.S. denotes no significant differences.

Results and Discussion

Modification and characterization of the AFMPs

The biocompatible poly(styrene-*co*-divinylbenzene) resin MPs used are commercially available hemoperfusion adsorption materials. Their average particle size was 1.26 ± 0.04 mm, due to which dropping debris into the peripheral blood circulation was improbable (Fig. S1(A) in the Electronic Supplementary Material (ESM)). To facilitate subsequent protein modification, we selected commercially available MPs containing free -COOH groups, and the Fourier-transform infrared (FTIR) spectra were employed to confirm the identity of these groups (Fig. S1(B) in the ESM). The MP morphology was characterized utilizing scanning electron microscopy. We found that the MP surfaces contained rough structures, which facilitated the availability of a larger area for the grafting of antibodies and capture of CTCs (Fig. S1(C) in the ESM). The traditional antibody modification method does not enable directional grafting onto the material surface, thus reducing the CTC-capturing efficiency of antibody-functionalized materials [28]. Hence, protein G was attached to the modification before antibody grafting, which can considerably improve the antibody grafting ratio and CTC capturing efficiency [45].

A thiol group on the surface of protein G was first activated with Traut's reagent (Fig. S2(A) in the ESM) and then coupled with NH_2–PEG–Mal. After the composite was grafted onto the surface of the untreated MPs, the nonspecific binding sites on the material surface were sealed with BSA (AMP). Finally, the anti-EpCAM antibody was incubated with and grafted onto the AFMP surface (Fig. 2(a)). The protein G surface after postthiolation had highly-exposed free thiol groups (Fig. S2(B) in the ESM). We chose a moderate concentration of Traut's reagent at 20 mg·mL^{-1} to prevent excessive thiolation which could structurally damage the protein G. We screened the incubation conditions best for thiolated protein G and PEG. PEG at 1 mg·mL^{-1} had the best effect when reacting with protein G for 4 h at room temperature (Fig. 2(b), Fig. S2(C) in the ESM). The degree of the reaction between the protein G complex and the MPs was also screened. When the concentration of the protein G complex was 0.25 mg·mL^{-1} (Fig. 2(c)), the grafting rate was maximal. However, when the concentration was increased further, the grafting efficiency gradually declined. Simultaneously, the grafting rate slowly reached a stable level with enhancing temperature and time (Fig. S2(D) in the ESM). The calibration curve for measuring the anti-EpCAM antibody concentration was plotted in the range of 0.001–10 mg·mL^{-1} (Fig. S3 in the ESM). The results revealed that, as Protein G is a class of IgG immunoglobulins that specifically recognizes and binds to crystallizable antibody fragments, it protects the activity of the antigen-binding antibody fragments, thereby enhancing the cell-capture ability of AFMPs. Compared with MPs directly coupled with the antibody, the protein G-modified MPs could generally enhance the grafting efficiency with a fluorescent antibody (Fig. 2(d)). It was the highest at 6 μg·mL^{-1}. Over time, the impact of antibody incubation gradually elevated at 37 °C. Considering antibody activity, we chose 12 h at 37 °C as the optimal antibody incubation conditions (Fig. 2(e)). Then the Alexa Fluo®647-conjugated EpCAM antibody was incubated with the antiphysical adsorption microsphere (AMP). The surface of the unmodified MP bore many antibodies due to its

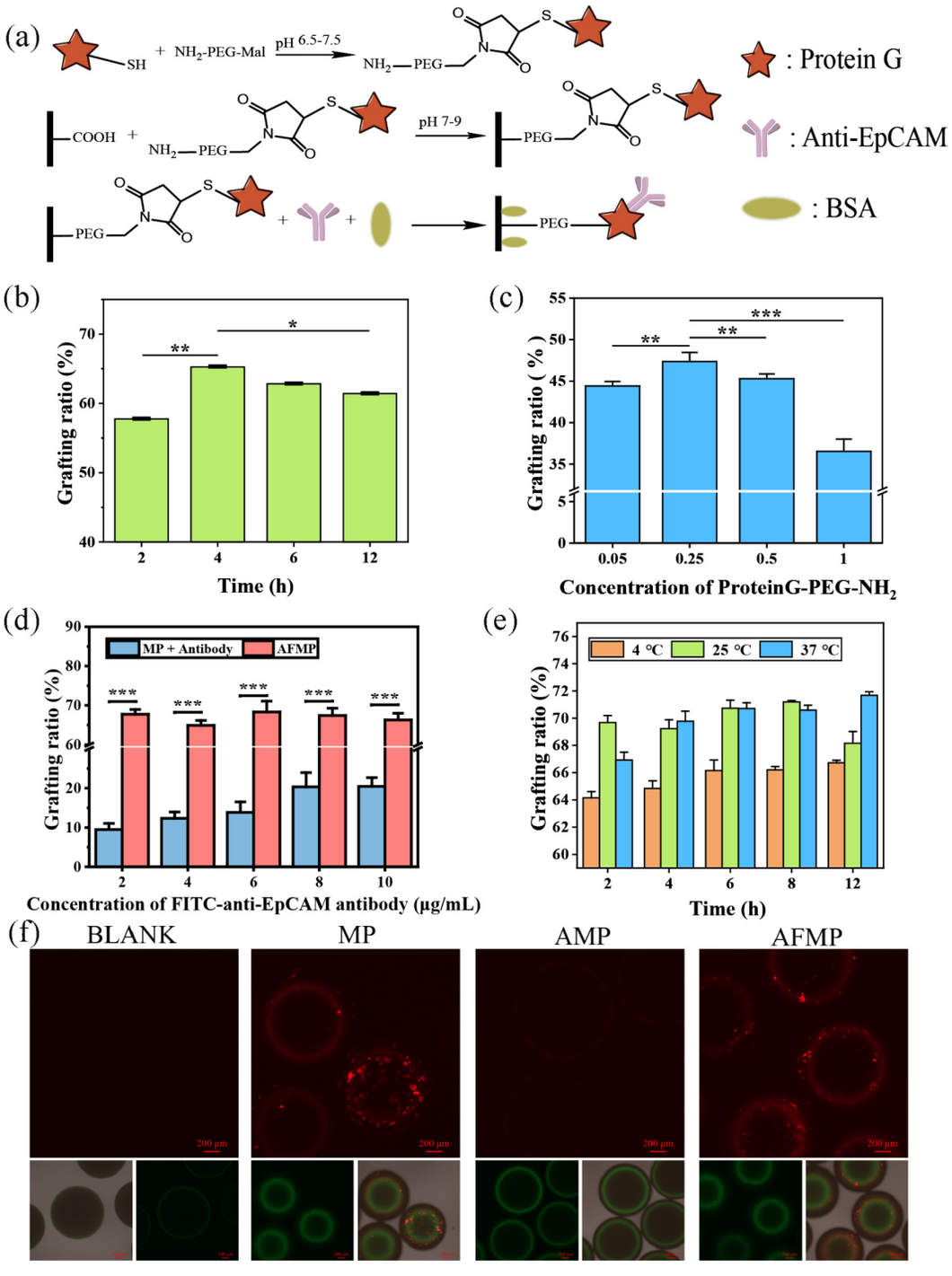

Fig. 2 Characterization of protein G and anti-EpCAM antibody grafting. **(a)** Synthetic steps involved in the conjugation of the anti-EpCAM antibody to the surface of the functionalized adsorbent. **(b)** The grafting ratio of protein G and Mal–PEG–NH_2 at 2, 4, 6, and 12 h. **(c)** The grafting ratio of protein G and 0.05, 0.25, 0.5, and 1 mg·mL^{-1} of the absorbent. **(d)** and **(e)** The grafting ratio of anti-EpCAM antibody (2, 4, 6, 8, and 10 μg·mL^{-1}) to the absorbent for different times (2, 4, 6, 8, and 10 h) and temperatures (4, 25, and 37 °C). **(f)** Confocal laser scanning microscopy (CLSM) images indicate the grafting affinity of the anti-EpCAM antibody with different functionalized adsorbents. Scale bar, 200 μm. Data are given as mean ± SD (n = 3 for each group), *p < 0.05, **p < 0.01, ***p < 0.001.

physical adsorption capability. After blocking with BSA, the levels of the antibody bound to the MP surface were markedly reduced. When the fluorescent-labeled antibody was incubated with the protein G-modified MP, the MP surface reexhibited red fluorescence, which indicated that this method could successfully modify the antibody on the AMP surface (Fig. 2(f)). 3D dynamic imaging also confirmed the uniform distribution of antibodies on the AMP surface (Movie S1 in the ESM).

CTCs captured statically *in vitro*

We mainly targeted EpCAM, which is highly expressed on the surface of CTCs, as a key marker for capturing them. To verify the effectiveness of the anti-EpCAM antibody-modified functional MPs for the specific capture of CTCs, we selected EpCAM-positive H1975 cells as CTC models and EpCAM-negative HeLa cells as controls. H1975 cells stained with DiD were coincubated with AFMPs (Fig. 3(a)). A large number of cells adhered to the surface of the unmodified MPs due to physical adsorption. After AMP treatment, the number of cells with nonspecific binding to the surface declined remarkably. After the AFMPs were coincubated with the model cells, the number of cells on the surface increased significantly, which confirmed the effectiveness of AFMP in capturing CTCs. After static incubation with the MPs, the size of the model cells on them increased properly (Fig. 3(b)). To evaluate the ability of AFMP to capture varying numbers of CTCs, the model cells were diluted to (2, 4, 6, 8, 10) × 10^4 and incubated with MPs in different groups. As shown in Fig. 3(c),

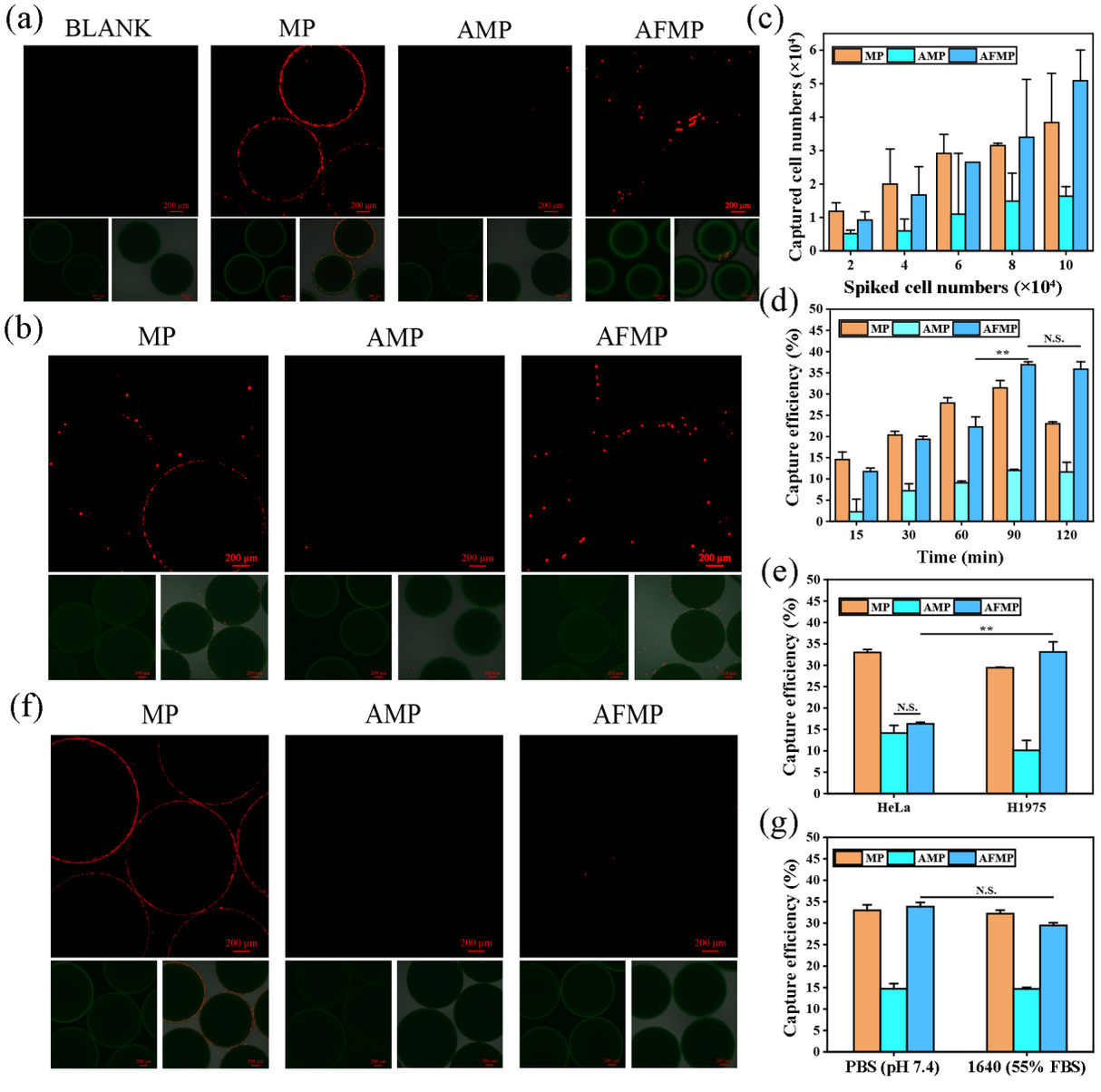

Fig. 3 Static CTC capture effect. **(a)** CLSM images showed that H1975 cells were captured by different functionalized adsorbents. Scale bar, 200 μm. **(b)** After a simple cleaning of the microspheres after capturing H1975 cells, the surface of the antibody-modified microspheres showed obvious cell retention. **(c)** Capture efficiency of the functionalized adsorbent for H1975 cells at (2, 4, 6, 8, 10) × 10^4 cells·mL^{-1}. **(d)** Capture efficiency of the functionalized adsorbent at 15, 30, 60, 90, and 120 min. **(e)** Capture efficiency of the different cell lines captured by the functionalized adsorbent. **(f)** CLSM images revealed that HeLa cells were rarely captured by the functionalized adsorbent. Scale bar, 200 μm. **(g)** Capture efficiency in different media. Data are given as mean ± SD (n = 3 for each group), N.S. not significant; **p < 0.01.

the ability of the AFMPs to capture the model cells gradually enhanced, and the capture rate was roughly colinear with the cell concentration (Fig. S4 in the ESM), proving the effectiveness of the MPs in capturing different amounts of CTCs. Similarly, compared with MPs directly coupled with the antibody, the protein G-modified MPs not only generally enhanced the grafting efficiency with the antibody but also successfully targeted the bound antibody, both of which contributed to the high H1975 cell capture efficiency of the AFMPs (Fig. S5 in the ESM). After determining the linear relationship between cell suspensions with different cell numbers and fluorescence intensities (Fig. S6 in the ESM), the model cells were incubated with the MPs for 15, 30, 60, 90, and 120 min to evaluate the ability of the AFMPs to capture CTCs at varied time points. The number of captured cells gradually increased with the incubation time until an optimal capture efficiency of 36.9% ± 0.66% at 90 min was reached (Fig. 3(d)). HeLa cells were used as models with low expression of EpCAM. The capture efficiency of the functionalized MPs varied markedly for the two cell types (Fig. 3(e)). The unmodified MPs had a robust nonspecific ability to adsorb HeLa and H1975 cells during static capture. The functionalized AFMPs could better capture specific H1975 cells compared with HeLa cells. Further, an investigation of the capture ability of the MPs through CLSM, revealed that they did not have any strong physical adsorption affinity with HeLa cells (Fig. 3(f)). This observation proved that the anti-EpCAM antibody-modified functional MPs have high specificity for capturing those tumor cells with elevated expression of EpCAM markers[37]. As an immunosorbent protein in the blood, IgG tends to wrap around the surface of foreign compounds, thus suppressing their adsorption in the blood. Considering that the capture efficiency fluctuates with incubation media, we used a medium containing 55% FBS to simulate the viscous and immune environment of human blood and investigated the capturing ability of the functional MPs. The results showed that, despite interference by viscosity, the immune proteins, and other factors, the AFMPs could still efficiently capture model cells in the simulated blood environment (Fig. 3(g)).

CTCs captured dynamically by PBCRD

The PBCRD comprised systems for CTC-capturing and returning purified blood into circulation. The CTC-capturing system consisted of anti-EpCAM antibody-modified functional MPs (AFMPs), and the other system comprised a peristaltic circulation pump for clinical blood perfusion and a blood catheter. (Fig. 4(a)). The 8.6 mm × 15.9 mm perfusion device with a volume of 1.0 mL was filled with the functional MPs. The volume could be adjusted according to the number of MPs (Fig. S7 in the ESM). Both ends of the removal device were connected to the matrix containing the CTC model cells with rubber hoses. When the peristaltic pump was started, the CTC model cells flowed along the rubber hose, from bottom to top in the removal device, and the other rubber hose to form a closed loop pathway. Thus, the CTCs could adequately contact the AFMP surface. H1975 model cells stained with DiD were also utilized for the dynamic CTC capture experiments. The unmodified MPs exhibited nonspecific adsorption during dynamic capture, allowing a significant percentage of nonspecific cells to cling to their surfaces (Fig. 4(b)). Only a few model cells were adsorbed on the surface of the AMPs due to certain properties of the material. However, the model cells could be easily captured by the surface of the AFMPs and would not detach due to specific recognition and high affinity. We also observed that the different-sized H1975 model cell clusters were captured by the AFMPs (Fig. S8 in the ESM). HeLa cells, a model cell type with negative EpCAM expression, demonstrated only partial adhesion onto the MP surface, while there was minimal cell adhesion on the AMP and AFMP surfaces (Fig. 4(c)). It was confirmed that the CTC model cells could be effectively captured by AFMP in the PBCRD, and the binding affinity of the antibody with the cells was affected by shear stress [46]. Similarly, the capture rate of H1975 model cells with elevated expression of EpCAM differed markedly from that of the HeLa model cells with low expression of EpCAM during the analysis of the PBCRD capture efficiency (Fig. 4(d)). When the cycle time of the PBCRD device was gradually enhanced to capture CTCs, the capture efficiency of the device gradually increased until the an optimal efficiency of 31.2% was reached at 30 min (Fig. 4(e)). When the circulation medium was replaced with a one containing 55% FBS to simulate the viscosity and immune conditions of human blood, the CTC model cells could still be efficiently captured by the AFMPs (Fig. 4(f)). Simultaneously, we also investigated the impact of different flow

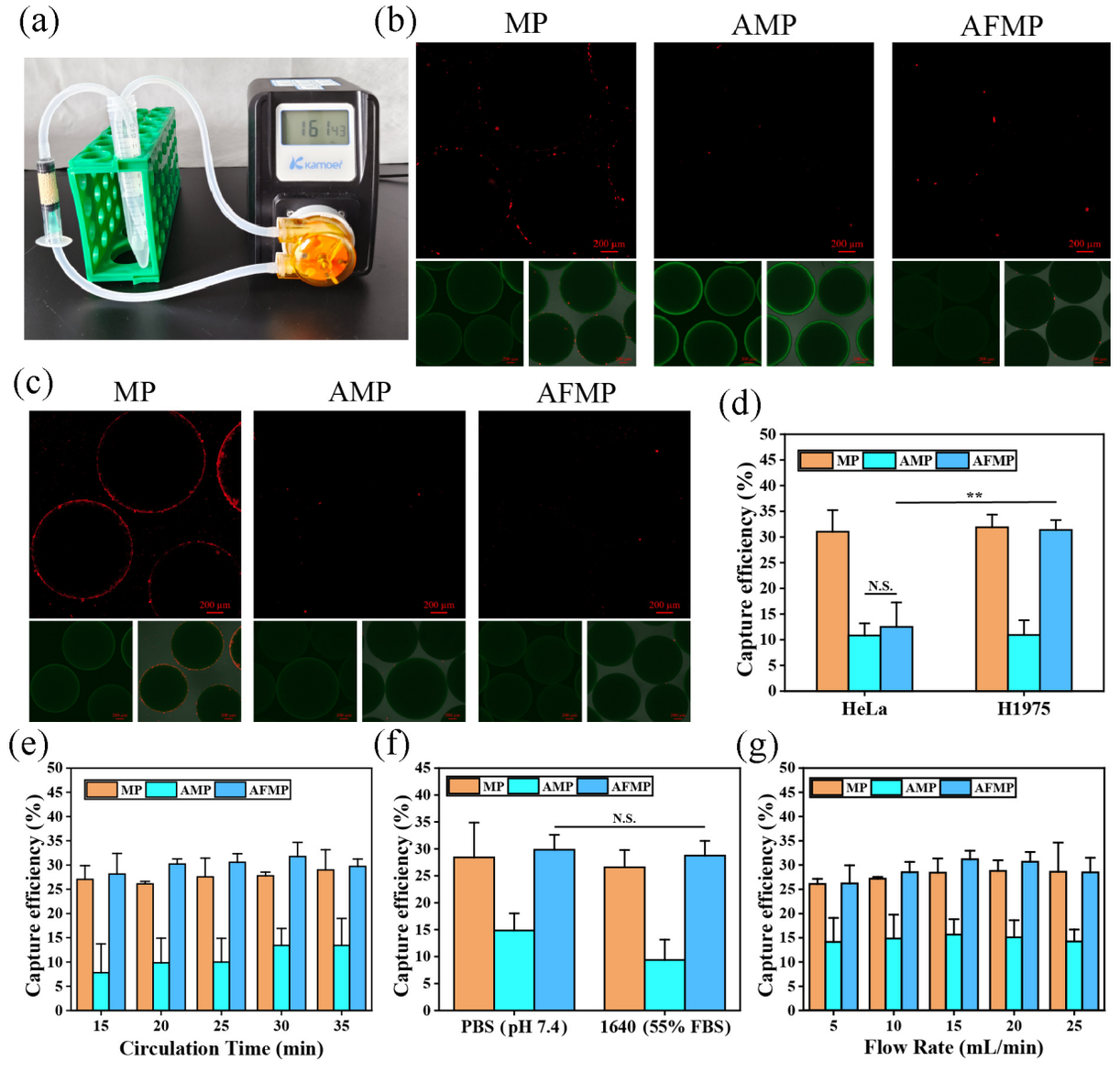

Fig. 4 Capture effect of CTCs with the Peripheral Blood CTC Removal Device. **(a)** Photographs of CTCs captured by the circulation device. **(b)** CLSM images showed that H1975 cells were captured by different functionalized adsorbents. Scale bar, 200 μm. **(c)** CLSM images indicated that HeLa cells were rarely captured by the functionalized adsorbent. Scale bar, 200 μm. **(d)** Capture efficiency of various cell lines captured by the functionalized adsorbent. **(e)** Capture efficiency of the PBCRD device at the circulation times of 15, 20, 25, 30, and 30 min. **(f)** Capture efficiency in different media. **(g)** Capture efficiency of the circulation device at the flow rates of 5, 10, 15, 20, and 25 mL·min^{-1}. Data are given as mean ± SD (n = 3 for each group), N.S. not significant; **p < 0.01.

velocities: 5, 10, 15, 20, and 25 mL·min^{-1} of the PBCRD on the dynamic capture efficiency of the AFMPs, and the best flow velocities were identified by calculating the cell capture efficiency of the CTC model (Fig. 4(g)). At 15 mL·min^{-1}, the capture efficiency was the highest (31.2%); because when the flow velocity decreased, the cycle index declined, which further resulted in lesser contact between the CTCs and the functionalized MPs; thus, fewer CTC model cells were captured successfully [47]. There were no significant differences in the CTCs captured by the MPs and AFMPs, mainly because the MPs physically adsorbed nonspecific cells which could not be dislodged by a high flow rate. The functionalized AFMPs could continuously capture specific CTCs while resisting the physical adsorption of nonspecific cells at enhanced flow rates. In addition, when the flow velocities were extreme, the shear stress of the circulating medium elevated, which enabled the easy detachment of the CTCs captured by the MPs. Further, the higher shear stress might have affected the cell morphology and thus their viability. Consequently, we chose a moderate flow velocity of 15 mL·min^{-1} to investigate the CTC capture ability of

the blood purifier.

CTCs captured by PBCRD during *in vivo* circulation

To further investigate the ability of the AFMPs to capture CTCs during blood circulation, SD rats were used as animal models to trap CTCs from blood circulation using the device. The blood was allowed to flow into the catheter of the PBCRD from the abdominal aorta of the rat. After purification with the PBCRD-containing functional MPs, the blood was returned to the inferior vena cava (Figs. 5(a) and 5(b), Movie S2 in the ESM). The cells were injected into the tail vein before the start of the cycle, and then the cells were captured in a cycle lasting 30 min. Before the PBCRD device starts circulation, the cells first enter the blood circulation of the rats before being processed through the system. The functionalized MPs were recycled post-circulation, and the cells captured on the MP surfaces were digested and removed. The RBCs were eliminated with a red blood cell lysate, and the remaining cells were stained with FITC-labeled CD45 antibody, Alexa Fluor®647-labeled EpCAM antibody, and DAPI (Fig. 5(c)). EpCAM-positive H1975 model cells could be captured on the AFMP surface. The DAPI-stained H1975 model cells were injected into the rat, and the clearance efficiency of AFMPs was ascertained based on the blood fluorescence levels, 20 min later (Fig. 5(d)). The autoimmune environment of the blood had a certain scavenging effect on CTCs [48], and ~10% of the CTCs could be cleared within 20 min. In contrast, the ordinary MPs adhered to the surfaces of a large number of immune cells and plasma proteins due to physical adsorption, due to which there was minuscule physical adsorption of CTCs on the MP

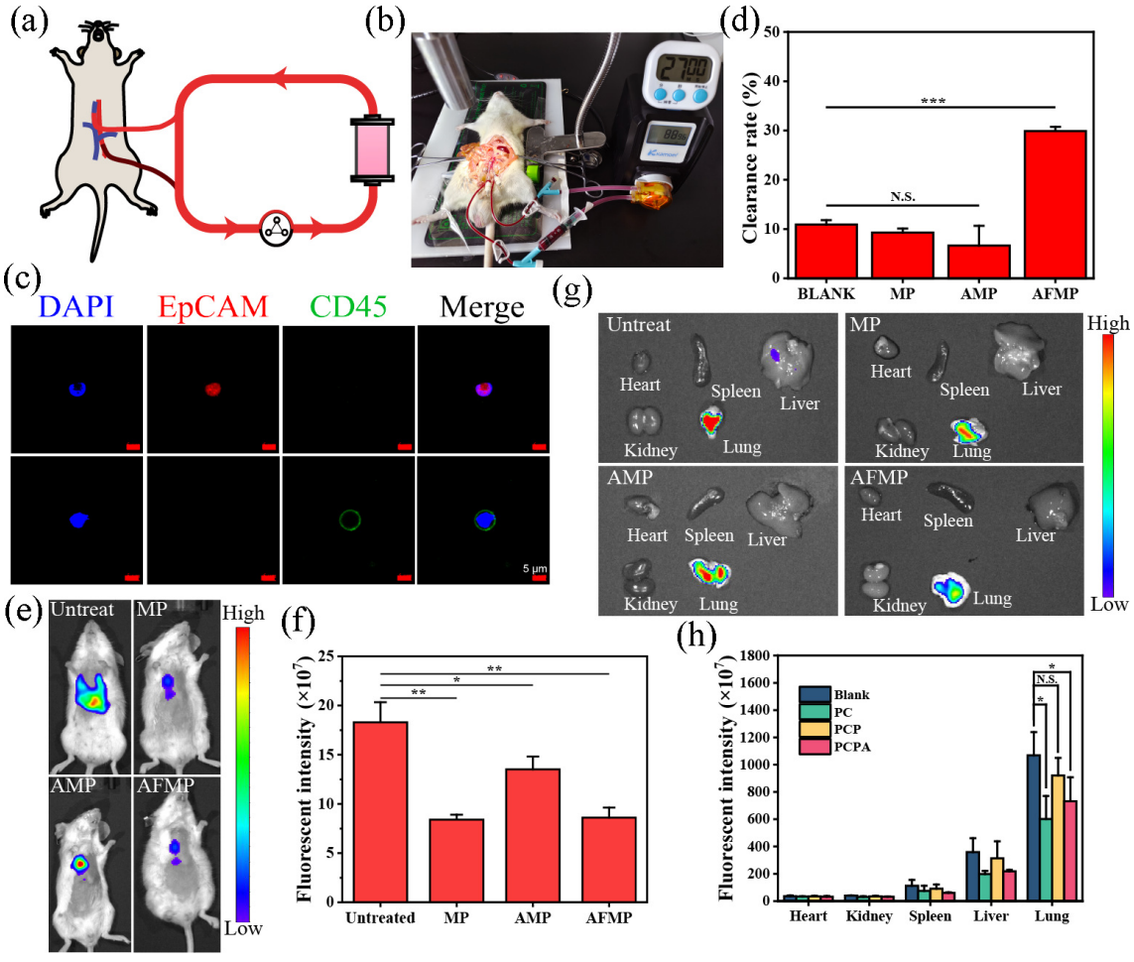

Fig. 5 Capture effect of CTCs in the animal model. **(a)** A schematic illustrating the rat circulatory model. **(b)** Photographs of CTC capturing in the rat circulatory model. **(c)** CLSM images of a H1975 cell (DAPI+/EpCAM$^+$/CD45$^-$) and a WBC (DAPI+/EpCAM$^-$/CD45$^+$) captured by antibody-modified functional microspheres. Scale bar, 200 μm. **(d)** Capture efficiency was determined based on the fluorescence value. **(e)** and **(f)** Fluorescent images of mice at 3 h after injection with treated CTCs indicate the average fluorescent intensity. **(g)** and **(h)** *Ex vivo* fluorescent images of mouse organs with the average fluorescent intensity. Data are given as mean ± SD (n = 3 for each group), N.S., not significant; *p < 0.05; **p < 0.01; ***p < 0.001.

surfaces in the model rats[49]. Because of their antiphysical adsorption properties, antibiosorption-modified microspheres (AMPs) had a very low ability to clear the model cells. In contrast, AFMPs had a remarkable capacity to clear CTCs (29.9% ± 0.82%).

To verify the reduction in residual cell retention in mice after cell capture by the PBCRD device and indirectly demonstrate the ability of the PBCRD device to inhibit tumor metastasis after CTC capture, mice were intravenously injected with the DIR-prestained H1975 cells, and the images were captured with an IVIS 3 h later (Figs. 5(e) and 5(f)). The tumor cells were first dynamically captured *in vitro* using the PBCRD device, and then the remaining cell suspension was injected into the mice via the tail vein. Therefore, the MPs still showed robust retention of CTCs *in vitro*, and the AMPs demonstrated similarly excellent resistance to physical adsorption. The average fluorescence intensity in the AFMP group mice was markedly lower than that in the control groups. Then, the mice were sacrificed, and the visceral images were captured by IVIS. Based on the comparisons of the average fluorescence intensity, the metastasis of CTCs *in vivo* could be effectively inhibited posttreatment with PBCRD utilizing AFMPs (Figs. 5(g) and 5(h)).

Biological safety of the AFMP

The raw material used was poly(styrene-*co*-divinylbenzene) resin MPs, the surface of which bore numerous -COOH groups, which reduced the pH of the medium. We first treated the cationic resin MPs with a sodium bicarbonate solution, neutralizing certain -COOH groups on the MP surfaces, and restoring the medium pH to the normal range. To investigate the biological safety of the prepared AFMPs, we conducted a biological safety inspection employing commercially available adsorption materials (Biosky) for blood perfusion. To investigate the impacts of the materials on the blood cell retention ratio, we first diluted fresh rat blood to a certain proportion and incubated it with the MP materials. The results showed that the untreated and unmodified MP surfaces had enhanced blood cell retention, and the blood cell retention rates of the AMP and AFMP were reduced significantly. Commercially available hemoperfusion adsorption materials also exhibited high nonspecific adsorption of blood cells (Fig. 6(a)). The model cells were mixed with the diluted blood cell suspension and then incubated with the MPs (Figs. S9 and S10 in the ESM). The blood cell retention rate was remarkably lesser than the CTC model cell capture rate by MPs. Unlike the nonspecific adsorption of different cells by the commercially available hemoperfusion adsorption materials, which resulted in low capture purity, AFMP demonstrated a higher efficiency in capturing CTC model cells as well as elevated capture purity. To verify the safety of the MPs in the RBCs, we incubated the prepared RBC suspension with the MPs to investigate their hemolytic efficiency (Fig. 6(b)). The results revealed that the MPs had excellent RBC compatibility and reached the same efficiency as commercially available blood perfusion adsorption materials. The cytotoxicity test showed that the AFMPs did not have any cytotoxic effects, which proved that they could be employed in the system to capture CTCs (Fig. 6(c)). The protein adsorption experiment also proved that the nonspecific adsorption of proteins onto the functionalized MPs was minute (Fig. 6(d)), which would not affect the blood circulatory protein levels.

To evaluate the *in vivo* biosafety and biocompatibility of the PBCRD in rats after hemoperfusion procedures, serum biochemical tests were performed on days 1, 7, and 14 postsurgery (Fig. 6(e), Fig. S11 in the ESM). The biochemical indices related to liver function, blood lipids, and total proteins returned to normal on day 14 after surgery. Routine blood tests revealed that white blood cell (WBC) and lymphocyte counts returned to normal on day 14 after surgery (Fig. 6(f), Fig. S12 in the ESM), and there were no remarkable quantitative alterations in the mean erythrocyte hemoglobin content or mean platelet volume, indicating that the AFMPs did not adhere robustly to the RBCs and platelets. In addition, the major organs on days 1 and 14 after surgery were sliced and stained with hematoxylin and eosin (Fig. 6(g)). The images showed that the inflammatory reaction caused by the surgery gradually subsided on day 14. Thus, these results demonstrated the excellent biocompatibility of AFMP *in vitro* and *in vivo*.

Discussion

A high CTC count was strongly associated with overall survival across multiple cancer types. The shedding of CTCs in patients with advanced malignancies and of tumor cells during the surgical excision of tumor tissues can trigger cancer

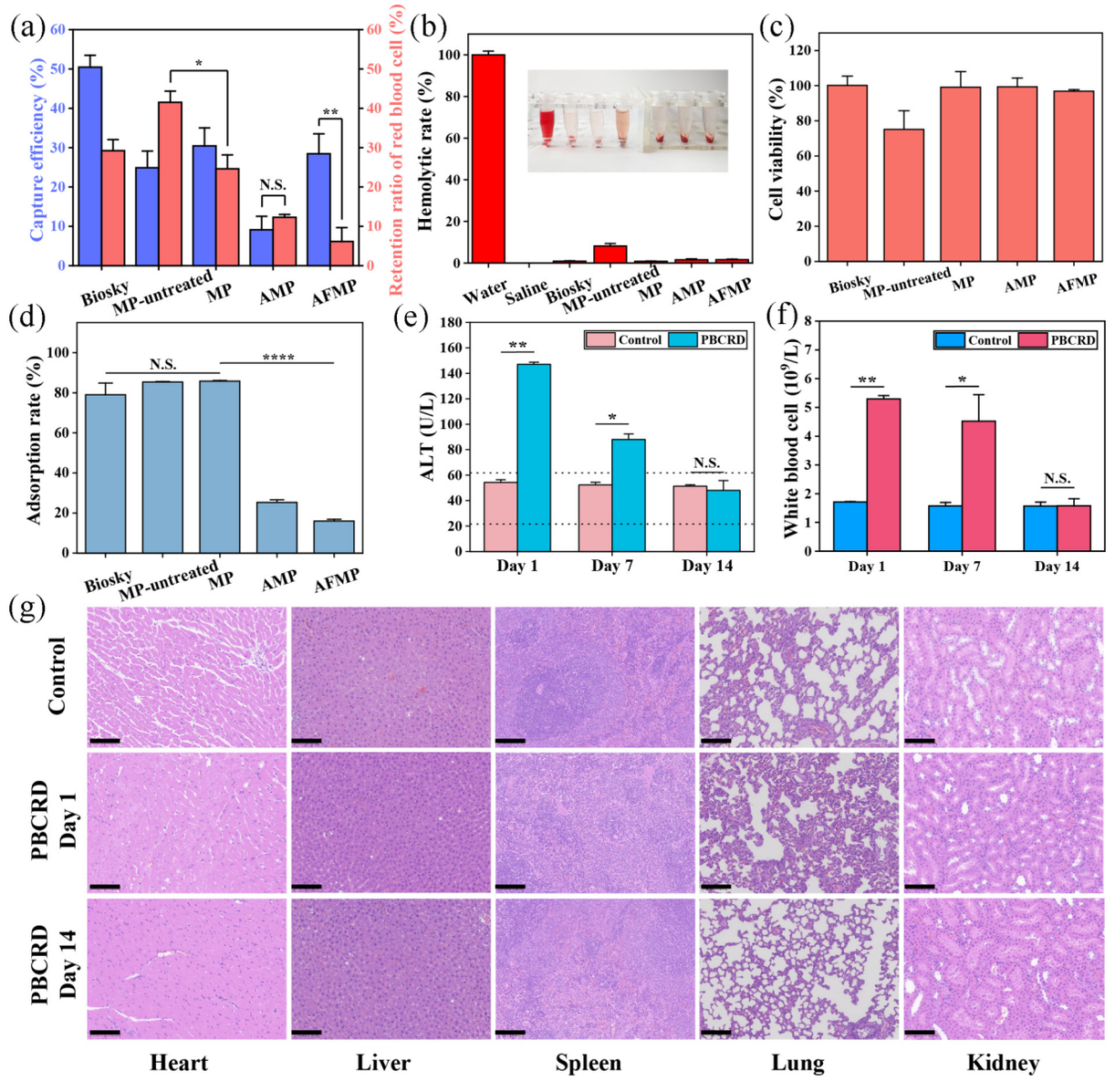

Fig. 6 Biocompatibility of the functionalized microspheres. **(a)** Comparison of the capture efficiency of CTCs and the red blood cell retention ratio. **(b)** Hemolytic rate of the modified functional microspheres. **(c)** Cytotoxicity of different functionalized microspheres to CTCs. **(d)** Protein adsorption rate of the different functionalized microspheres. **(e)** Serum biochemical indices related to liver function of the rat after surgery at days 1, 7, and 14. **(f)** White blood cell analysis after surgery at days 1, 7, and 14. **(g)** H&E staining of the heart, liver, spleen, lungs, and kidneys after surgery on days 1 and 14. Scale bar, 100 μm. Data are given as mean ± SD (n = 3 for each group), N.S., not significant; *p < 0.05; **p < 0.01; ****p < 0.000 1.

metastasis and recurrence [6–8]. The detection and counting of CTCs have emerged as a very promising technique for cancer diagnosis and are increasingly being applied in commercial cancer detection strategies [5, 11]. However, methods such as liquid biopsy for CTCs are limited by the number of CTCs, resulting in false negatives, and also are unable to capture and remove CTCs from the systemic circulation to inhibit tumor metastasis [40–42], which largely hinders their clinical applicability. Introducing a blood purification model into CTC research is a considerable advancement. Such a strategy can be applied to capture and remove CTCs in the blood as well as effectively alleviate or prevent the metastasis of CTCs to other organs and further deterioration, which has potential therapeutic importance.

By leveraging the capability of the blood purification systems to remove harmful compounds from the blood, the adsorbent material utilized in the blood purification system can be further modified to capture CTCs from circulating blood. During the purification of antibodies by immunoaffinity

chromatography, protein G can specifically recognize the crystallizable fragment of the antibody, thus ensuring the activity and efficiency of the antibodies in capturing CTCs [28, 45]. Therefore, protein G was first added on the surface of the adsorbent MPs, and then an anti-EpCAM antibody was directionally modified on the surface of the MPs. By taking advantage of the high expression of EpCAM markers on the surface of CTCs, CTCs in the blood can be bound with AFMP and enriched. By blocking the physical binding sites on the MP surfaces with BSA, the adsorption of blood cells and proteins can be effectively prevented. In the recent research on the capture of CTCs from peripheral circulation, the capture efficiency of CTCs was only 2%, with a relatively low capture purity [37, 38]. PBCRD can effectively enhance the efficiency and purity of CTCs captured from the peripheral circulation. In the PBCRD experiments performed using simulated blood circulation, AFMPs could capture >31% ± 1.76% of the CTC model cells at a high flow rate of 15 mL·min^{-1}.

In the rat blood circulation model, PBCRD comprising AFMP was able to capture CTCs, which indicates that the PBCRD constructed in this study may potentially be developed into a clinical adjuvant therapy for inhibiting tumor metastasis. CTCs are employed as biomarkers for early cancer screening, clinical staging, cancer-type diagnosis, and recurrence monitoring [50]. The clinical value of CTCs has been proven in research on the metastasis of breast [51], lung [52, 53], and colorectal cancers [54]. The extensive enrichment of CTCs from the peripheral circulation further expanded their clinical applicability in combination with the sequencing of downstream genes and characteristic molecular analysis. However, epithelial–mesenchymal transition (EMT) generally occurs when tumor cells enter the peripheral blood [55], which is crucial for their survival during their movement from the primary tumor to the colonization site under severe conditions. EMT changes or eliminates the epithelial phenotype markers of CTCs and causes them to present a high degree of heterogeneity. Therefore, approaches based on EpCAM could not be employed to detect CTCs with low EpCAM expression and of nonepithelial phenotype [56, 57]. Thus, this analysis may underestimate the importance of CTCs undergoing EMT during tumor proliferation and metastasis. This study verified the effectiveness of an anti-EpCAM antibody-functionalized blood purification system in capturing epithelial CTCs. However, the AFMPs used in the PBCRD only demonstrated <31% ± 1.76% efficiency in clearing CTCs in the rat blood circulation model. Thus, this approach has certain limitations in inhibiting tumor metastasis caused by CTC metastasis. The efficiency of CTC capture from the blood can be improved by further modifying the MPs and optimizing the capture conditions, such as the flow volume, in subsequent studies. Based on the variations in the expression of the surface markers on mesenchymal and mixed epithelial–mesenchymal CTCs, we can further modify the antibodies related to epithelial and mesenchymal biomarkers on the MPs or mix modified functional MPs with different antibodies to capture and clear a variety of heterogeneous CTCs simultaneously. This approach is expected to play a more profound role in cancer treatment. In addition, to further promote the clinical applicability and commercialization of this approach, its safety and biocompatibility should be investigated further.

Conclusions

We present for the first time, the application of antibody modification employing an immunosorbent material in combination with PBCRD for the capture of CTCs in a high-throughput, peripheral blood circulation environment. This approach enabled the efficient capture of CTCs in large-volume blood circulation. The successful capture of CTCs was confirmed in rat circulation capture experiments, and by using a mouse retention model to capture CTCs to show that the strategy could effectively inhibit the metastasis of CTCs. The AFMPs had excellent bio and blood compatibility and showed no obvious side effects on vital organs, indicating the applicability of AFMPs for the elimination of CTCs from blood *in vivo*. In subsequent studies, we can further modify the antibodies/aptamers related to the epithelial and mesenchymal biomarkers on the MPs or combine the modified functional MPs with different antibodies/aptamers to simultaneously capture and clear a variety of heterogeneous CTCs. Overall, the model combining AFMPs with PBCRD greatly improved the efficiency of CTC capture from the peripheral circulation, which can effectively inhibit tumor metastasis and progression, providing a completely

new pathway for clinical therapies to remove CTCs for antimetastatic purposes.

CRediT Author Statement

Jun Luo, **Lei Xing**, **Ming-Tao Yu**, and **Hu-Lin Jiang**: conceptualization, writing–review, and editing. **Lei Xing and Hu-Lin Jiang**: project administration and supervision. **Jun Luo**, **Ming-Tao Yu, Ying Sun**, **Wen-Jia Wang**, **Xiao-Jie Wang**, and **Yang-Ze Ji**: Data curation. **Jun Luo**, **Ying Sun**, **and Ming-Tao Yu:** analysis and investigation. Xing Wan, Yi Wang, and Tian-Jiao Zhou: methodology. All authors discussed and edited the manuscript.

Ethics Approval Statement

The animal experiments was examined and approved by the Animal Ethics Committee of China Pharmaceutical University (Approval ID: 2021-04-003).

Acknowledgements

This work was financially supported by the National Natural Science Foundation of China (82020108029, 82473867, 82302367, 82304416). This work was also supported by the Natural Science Foundation of Jiangsu Province (BK20231016, BK20231019), the Natural Science Foundation of Jiangsu Basic Research Program-Project jointly funded by province and city (BK20232035), State Key Laboratory of Natural Medicines China Pharmaceutical University (SKLNMZZ202021), Double First-class University Projects (CPU2018GY06) and Double First-Rate construction plan of China Pharmaceutical University (CPU2022QZ18).

Conflict of Interests

The authors declare that they have no known competing financial interests or personal relationships that could have appeared to influence the work reported in this paper.

Supporting Information

Supporting information to this article can be found online at https://doi.org/10.26599/NBE.2025.9290114

References

[1] F. Bray, M. Laversanne, H. Sung, et al. Global cancer statistics 2022: GLOBOCAN estimates of incidence and mortality worldwide for 36 cancers in 185 countries. *CA*, 2024, 74(3): 229–263. https://doi.org/10.3322/caac.21834

[2] C.L. Chaffer, R.A. Weinberg. A perspective on cancer cell metastasis. *Science*, 2011, 331(6024): 1559−1564. https://doi.org/10.1126/science.1203543

[3] Y. Zheng, Y. Han, Q. Sun, et al. Harnessing anti-tumor and tumor-tropism functions of macrophages *via* nanotechnology for tumor immunotherapy. *Exploration*, 2022, 2(3): 20210166. https://doi.org/10.1002/EXP.20210166

[4] S.D. Nathanson, M. Detmar, T.P. Padera, et al. Mechanisms of breast cancer metastasis. *Clinical & Experimental Metastasis*, 2022, 39(1): 117−137. https://doi.org/10.1007/s10585-021-10090-2

[5] H. Esmaeilsabzali, T.V. Beischlag, M.E. Cox, et al. Detection and isolation of circulating tumor cells: Principles and methods. *Biotechnology Advances*, 2013, 31(7): 1063−1084. https://doi.org/10.1016/j.biotechadv.2013.08.016

[6] T.N. Seyfried, L.C. Huysentruyt. On the origin of cancer metastasis. *Critical Reviews in Oncogenesis*, 2013, 18(1-2): 43−73. https://doi.org/10.1615/critrevoncog.v18.i1-2.40

[7] A.W. Lambert, D.R. Pattabiraman, R.A. Weinberg. Emerging biological principles of metastasis. *Cell*, 2017, 168(4): 670−691. https://doi.org/10.1016/j.cell.2016.11.037

[8] D.F. Lin, L.S. Shen, M. Luo, et al. Circulating tumor cells: Biology and clinical significance. *Signal Transduction and Targeted Therapy*, 2021, 6: 404. https://doi.org/10.1038/s41392-021-00817-8

[9] M. Cristofanilli, G.T. Budd, M.J. Ellis, et al. Circulating tumor cells, disease progression, and survival in metastatic breast cancer. *Asian Pacific Journal of Cancer Prevention*, 2004, 351(8): 781−791. https://doi.org/10.1056/NEJMoa040766

[10] O.A. Martin, R.L. Anderson, K. Narayan, et al. Does the mobilization of circulating tumour cells during cancer therapy cause metastasis. *Nature Reviews Clinical Oncology*, 2017, 14(1): 32−44. https://doi.org/10.1038/nrclinonc.2016.128

[11] G. Awiaz, J. Lin, A. Wu. Recent advances of Au@Ag core-shell SERS-based biosensors. *Exploration*, 2023, 3(1): 20220072. https://doi.org/10.1002/EXP.20220072

[12] J. Chen, L.X. Yu, Y. Li, et al. Biospecific monolayer coating for multivalent capture of circulating tumor cells with high sensitivity. *Advanced Functional Materials*, 2019, 29(33): 1808961. https://doi.org/10.1002/adfm.201808961

[13] Y. Song, Y. Shi, M. Huang, et al. Bioinspired engineering of a multivalent aptamer-functionalized nanointerface to enhance the capture and release of circulating tumor cells. *Angewandte Chemie International Edition*, 2019, 58(8): 2236−2240. https://doi.org/10.1002/anie.201809337

[14] M.R. Sun, J.S. Xu, J.G. Shamul, et al. Creating a capture zone in microfluidic flow greatly enhances the throughput and efficiency of cancer detection. *Biomaterials*, 2019, 197: 161−170. https://doi.org/10.1016/j.biomaterials.2019.01.014

[15] M. Tang, H.F. Xia, C.M. Xu, et al. Magnetic chip based

extracorporeal circulation: A new tool for circulating tumor cell *in vivo* detection. *Analytical Chemistry*, 2019, 91(23): 15260−15266. https://doi.org/10.1021/acs.analchem.9b04286

[16] Y. Xie, D. Chen, S.J. Lin. Microfluidic electrochemical detection techniques of cancer biomarkers. *Nano Biomedicine and Engineering*, 2017, 9(1): 57−71. https://doi.org/10.5101/nbe.v9i1.p57-71

[17] A. Mishra, T.D. Dubash, J.F. Edd, et al. Ultrahigh-throughput magnetic sorting of large blood volumes for epitope-agnostic isolation of circulating tumor cells. *Proceedings of the National Academy of Sciences of the United States of America*, 2020, 117(29): 16839−16847. https://doi.org/10.1073/pnas.2006388117

[18] D.K. Ye, M. Li, T.T. Zhai, et al. Encapsulation and release of living tumor cells using hydrogels with the hybridization chain reaction. *Nature Protocols*, 2020, 15: 2163−2185. https://doi.org/10.1038/s41596-020-0326-4

[19] L. Zhu, X.Q. Feng, S.H. Yang, et al. Colorimetric detection of immunomagnetically captured rare number CTCs using mDNA-wrapped single-walled carbon nanotubes. *Biosensors and Bioelectronics*, 2021, 172: 112780. https://doi.org/10.1016/j.bios.2020.112780

[20] D. Huh, J.H. Bahng, Y. Ling, et al. Gravity-driven microfluidic particle sorting device with hydrodynamic separation amplification. *Analytical Chemistry*, 2007, 79(4): 1369−1376. https://doi.org/10.1021/ac061542n

[21] J.V. Green, S.K. Murthy. Microfluidic enrichment of a target cell type from a heterogenous suspension by adhesion-based negative selection. *Lab on a Chip*, 2009, 9(15): 2245. https://doi.org/10.1039/b906768j

[22] M. Hosokawa, T. Hayata, Y. Fukuda, et al. Size-selective microcavity array for rapid and efficient detection of circulating tumor cells. *Analytical Chemistry*, 2010, 82(15): 6629−6635. https://doi.org/10.1021/ac101222x

[23] V. J. Hofman, M.I. Ilie, C. Bonnetaud, et al. Cytopathologic detection of circulating tumor cells using the isolation by size of epithelial tumor cell method: Promises and pitfalls. *Journal of the American Chemical Society*, 2011, 135(1): 146−156. https://doi.org/10.1309/AJCP9X8OZBEIQVVI

[24] L.S. Lim, M. Hu, M.C. Huang, et al. Microsieve lab-chip device for rapid enumeration and fluorescence *in situ* hybridization of circulating tumor cells. *Lab on a Chip*, 2012, 12(21): 4388. https://doi.org/10.1039/c2lc20750h

[25] J.M. Park, J.Y. Lee, J.G. Lee, et al. Highly efficient assay of circulating tumor cells by selective sedimentation with a density gradient medium and microfiltration from whole blood. *Analytical Chemistry*, 2012, 84(17): 7400−7407. https://doi.org/10.1021/ac3011704

[26] L.L. Wu, H.M. Ding, X. Qu, et al. Fluidic multivalent membrane nanointerface enables synergetic enrichment of circulating tumor cells with high efficiency and viability. *Journal of the American Chemical Society*, 2020, 142(10): 4800−4806. https://doi.org/10.1021/jacs.9b13782

[27] S. Riethdorf, L. O'Flaherty, C. Hille, et al. Clinical applications of the CellSearch platform in cancer patients. *Advanced Drug Delivery Reviews*, 2018, 125: 102−121. https://doi.org/10.1016/j.addr.2018.01.011%20Get%20rights%20and%20content

[28] A. Seyfoori, S.A. Seyyed Ebrahimi, E. Samiei, et al. Multifunctional hybrid magnetic microgel synthesis for immune-based isolation and post-isolation culture of tumor cells. *ACS Applied Materials & Interfaces*, 2019, 11(28): 24945−24958. https://doi.org/10.1021/acsami.9b02959

[29] X.J. Ma, W.Q. Yang, X. Ge, et al. Design a novel multifunctional ($CsPbBr_3$/Fe_3O_4)@MPSs@SiO_2 magneto-optical microspheres for capturing circulating tumor cells. *Applied Surface Science*, 2021, 551: 149427. https://doi.org/10.1016/j.apsusc.2021.149427

[30] C. Li, S. Yang, R. Li, et al. Dual-aptamer-targeted immunomagnetic nanoparticles to accurately explore the correlations between circulating tumor cells and gastric cancer. *ACS Applied Materials & Interfaces*, 2022, 14(6): 7646−7658. https://doi.org/10.1021/acsami.1c22720

[31] E. Lin, L. Rivera-Báez, S. Fouladdel, et al. High-throughput microfluidic labyrinth for the label-free isolation of circulating tumor cells. *Cell Systems*, 2017, 5(3): 295−304.e4. https://doi.org/10.1016/j.cels.2017.08.012

[32] M.F. Abate, S. Jia, M.G. Ahmed, et al. Visual quantitative detection of circulating tumor cells with single-cell sensitivity using a portable microfluidic device. *Small*, 2019, 15(14): e1804890. https://doi.org/10.1002/smll.201804890

[33] Y.H. Cheng, Y.C. Chen, E. Lin, et al. Hydro-Seq enables contamination-free high-throughput single-cell RNA-sequencing for circulating tumor cells. *Nature Communications*, 2019, 10: 2163. https://doi.org/10.1038/s41467-019-10122-2

[34] J.J. Shi, C.Q. Zhao, M.Q. Shen, et al. Combination of microfluidic chips and biosensing for the enrichment of circulating tumor cells. *Biosensors and Bioelectronics*, 2022, 202: 114025. https://doi.org/10.1016/j.bios.2022.114025

[35] T.H. Kim, Y. Wang, C.R. Oliver, et al. A temporary indwelling intravascular aphaeretic system for *in vivo* enrichment of circulating tumor cells. *Nature Communications*, 2019, 10: 1478. https://doi.org/10.1038/s41467-019-09439-9

[36] S.B. Cheng, M. Wang, C. Zhang, et al. Flexible three-dimensional net for intravascular fishing of circulating tumor cells. *Analytical Chemistry*, 2020, 92(7): 5447−5455. https://doi.org/10.1021/acs.analchem.0c00203

[37] D. Wang, C. Ge, W. Liang, et al. *In vivo* enrichment and elimination of circulating tumor cells by using a black phosphorus and antibody functionalized intravenous catheter. *Advanced Science*, 2020, 7(17): 2000940. https://doi.org/10.1002/advs.202000940

[38] D. Wang, R.H. Dong, X.D. Wang, et al. Flexible electronic catheter based on nanofibers for the *in vivo* elimination of circulating tumor cells. *ACS Nano*, 2022, 16(4): 5274−5283. https://doi.org/10.1021/acsnano.1c09807

[39] A. Ilyas, W. Asghar, Y.T. Kim, et al. Parallel recognition of cancer cells using an addressable array of solid-state micropores. *Biosensors and Bioelectronics*, 2014, 62: 343−349. https://doi.org/10.1016/j.bios.2014.06.048

[40] A. Jakabova, Z. Bielcikova, E. Pospisilova, et al. Characterization of circulating tumor cells in early breast cancer patients receiving neoadjuvant chemotherapy. *Therapeutic Advances in Medical Oncology*, 2021, 13: 17588359211028492. https://doi.org/10.1177/17588359211028492

[41] Z. Kejík, R. Kaplánek, P. Dytrych, et al. Circulating tumour cells (CTCs) in NSCLC: From prognosis to therapy design. *Pharmaceutics*, 2021, 13(11): 1879. https://doi.org/10.3390/pharmaceutics13111879

[42] X. Weng, D. Wei, Z. Yang, et al. Photodynamic therapy reduces metastasis of breast cancer by minimizing circulating tumor cells. *Biomedical Optics Express*, 2021, 12(7): 3878−3886. https://doi.org/10.1364/BOE.429947

[43] Y.M. Chai, Z. Liu, Y.Z. Du, et al. Hydroxyapatite reinforced inorganic-organic hybrid nanocomposite as high-performance adsorbents for bilirubin removal *in vitro* and in pig models. *Bioactive Materials*, 2021, 6(12): 4772−4785. https://doi.org/10.1016/j.bioactmat.2021.05.

017
[44] A. Tyagi, Y.W. Ng, M. Tamtaji, et al. Elimination of uremic toxins by functionalized graphene-based composite beads for direct hemoperfusion. *ACS Appl Mater Interfaces*, 2021, 13(5): 5955−5965. https://doi.org/10.1021/acsami.0c19536
[45] Y. Jung, J.M. Lee, H. Jung, et al. Self-directed and self-oriented immobilization of antibody by protein G-DNA conjugate. *Analytical Chemistry*, 2007, 79(17): 6534−6541. https://doi.org/10.1021/ac070484i
[46] B. Kwak, J. Lee, J. Lee, et al. Spiral shape microfluidic channel for selective isolating of heterogenic circulating tumor cells. *Biosensors and Bioelectronics*, 2018, 101: 311−316. https://doi.org/10.1016/j.bios.2017.10.036
[47] H.W. Hou, M.E. Warkiani, B.L. Khoo, et al. Isolation and retrieval of circulating tumor cells using centrifugal forces. *Scientific Reports*, 2013, 3: 1259. https://doi.org/10.1038/srep01259
[48] E.Z. Keung, J.A. Wargo. The current landscape of immune checkpoint inhibition for solid malignancies. *Surgical Oncology Clinics of North America*, 2019, 28(3): 369−386. https://doi.org/10.1016/j.soc.2019.02.008
[49] S.A. Shah. Participation of the immune system in regression of a rat Mc7 sarcoma by hyperthermia. *Cancer Research*, 1981, 41(5): 1742−1747.
[50] V. Appierto, S. Di Cosimo, C. Reduzzi, et al. How to study and overcome tumor heterogeneity with circulating biomarkers: The breast cancer case. *Seminars in Cancer Biology*, 2017, 44: 106−116. https://doi.org/10.1016/j.semcancer.2017.04.007
[51] M.J.M. Magbanua, C. Yau, D.M. Wolf, et al. Synchronous detection of circulating tumor cells in blood and disseminated tumor cells in bone marrow predicts adverse outcome in early breast cancer. *Clinical Cancer Research*, 2019, 25(17): 5388−5397. https://doi.org/10.1158/1078-0432.CCR-18-3888
[52] J.M. Hou, M. Krebs, T. Ward, et al. Circulating tumor cells as a window on metastasis biology in lung cancer. *The American Journal of Pathology*, 2011, 178(3): 989−996. https://doi.org/10.1016/j.ajpath.2010.12.003
[53] M. Ilié, E. Szafer-Glusman, V. Hofman, et al. Detection of PD-L1 in circulating tumor cells and white blood cells from patients with advanced non-small-cell lung cancer. *Annals of Oncology*, 2018, 29(1): 193−199. https://doi.org/10.1093/annonc/mdx636
[54] L.R. Jiao, C. Apostolopoulos, J. Jacob, et al. Unique localization of circulating tumor cells in patients with hepatic metastases. *Journal of Clinical Oncology*, 2009, 27(36): 6160−6165. https://doi.org/10.1200/jco.2009.24.5837
[55] M.Ø. Agerbæk, S.R. Bang-Christensen, M.H. Yang, et al. The VAR2CSA malaria protein efficiently retrieves circulating tumor cells in an EpCAM-independent manner. *Nature Communications*, 2018, 9: 3279. https://doi.org/10.1038/s41467-018-05793-2
[56] P.K. Grover, A.G. Cummins, T.J. Price, et al. Circulating tumour cells: The evolving concept and the inadequacy of their enrichment by EpCAM-based methodology for basic and clinical cancer research. *Annals of Oncology*, 2014, 25(8): 1506−1516. https://doi.org/10.1093/annonc/mdu018
[57] X.J. Wang, Y.Z. Ji, J. Luo, et al. An advanced multivalent ligand-decorated microsphere enrichment system efficiently captures circulating tumor cells *in vivo*. *Small*, 2025: 2409036. https://doi.org/10.1002/smll.202409036